Single dopant nanowire transistors: influence of phonon scattering and temperature

H. Carrillo-Nuñez*†, M. Bescond*, E. Dib*, N. Cavassilas*, and M. Lannoo*
*IM2NP, UMR CNRS 7334, Bat. IRPHE, 13384 Marseille, France
†Integrated Systems Laboratory ETH Zürich, Gloriastrasse 35, 8092 Zürich, Switzerland
e-mail: marc.bescond@im2np.fr

***Abstract*—A three-dimensional self-consistent non-equilibrium Green's function approach is used to investigate the influence of phonon scattering in single dopant nanowire transistors. Phonon interactions are described within the self-consistent Born approximation in which both acoustic and optical phonons are included. Transport properties are then analyzed in the ballistic and scattering regimes. Ballistic results first confirm the current hysteresis due to two different screening mechanisms of the dopant reported by Mil'nikov *et-al* [1]. The transition between them is smoothed by the interactions with acoustic phonons which suppress the current hysteresis. Interestingly our findings also show a beneficial impact of the optical phonon interactions. They generate a phonon-assisted resonant tunneling from which can result a higher current than in the ballistic regime. Finally a temperature dependance analysis shows that the hysteresis should be restored at lower temperatures.**

I. Introduction

Thanks to recent technological developments, single–atom electronics is now conceivable. So far very few works, whether experimental [2] or theoretical [3], focused on new applications with single dopant semiconductor devices at room temperature. In that context, simulations performed by Mil'nikov *et-al* predicted a remarkable intrinsic bistability in single dopant nanowire Metal-Oxide-Semiconductor (MOS) transistor [1]. This bistability results from two distinct screening mechanisms of the Coulomb potential impurity and could lead to relevant applications. However the study only considers the ballistic regime and optical-phonon interactions in the scope of the resonant tunneling model [4].

In this work, quantum transport simulations are performed *via* a three dimensional real–space non-equilibrium Green's function (NEGF) approach. Both acoustic- and optical-phonon interactions are tackled within the self-consistent Born approximation [5], which represents one of the most suited model to include scattering in nano-devices. Based on this approach, we investigate the influence of phonon interactions on electron transport through a single dopant nanowire transistor. A temperature dependance analysis is also performed.

The paper is organized as follows: Section II gives the main features of the theoretical approach for the 3D-NEGF and SCBA formalisms. In section III, we investigate in detail the impact of phonon scattering in a single dopant nanowire MOSFET. The suppression of bistability and the influence of phonon-assisted resonant tunneling are discussed by analyzing separately acoustic and optical phonons. Eventual restoration of the hysteresis at lower temperatures is also discussed. The conclusions of our work are given in section IV.

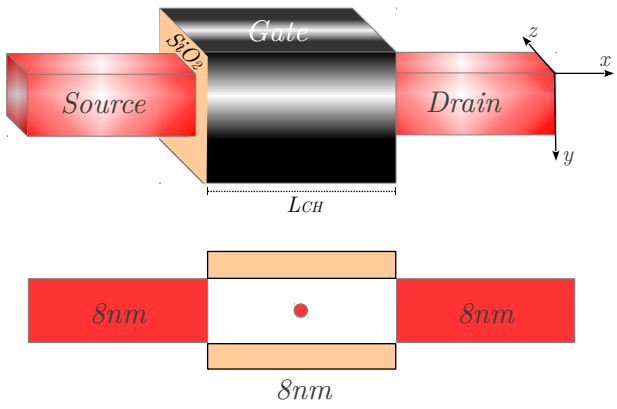

Fig. 1. Representation of the considered silicon nanowire transistor with dopant located at the center of the channel. The silicon cross-section is 2×2 nm^2 and L_{CH}=8 nm. In all the study source/drain doping is N_D=10^{20}cm^{-3} and transport direction is <100>.

II. Simulation details

We consider the n-type silicon gate-all-around (GAA) MOSFET sketched in Fig. 1. Source, channel and drain regions are 8 nm long each. The channel is intrinsic and its crystallographic orientation is along the <100> direction. Transport properties are calculated based on the 3D real-space NEGF approach expressed within the effective mass approximation. Hard wall boundary conditions are assumed. The hamiltonian is then projected on a 3D grid with a real-space mesh equals to 0.2 nm and an energy interval of 1 meV. Both acoustic and optical phonon couplings are considered and described within a local approximation. For a given valley ν of the conduction band, the general SCBA electron–phonon self–energy is defined as [6]–[8]

$$\Sigma^{\lessgtr}_{S,\nu}(E) = \sum_{\nu'}\sum_{q}\left|M_q^{\nu,\nu'}\right|^2\Big[\eta_q G^{\lessgtr}_{\nu'}(E\mp\hbar\omega_q) + (\eta_q+1)G^{\lessgtr}_{\nu'}(E\pm\hbar\omega_q)\Big], \quad (1)$$

where $\hbar\omega_q$, $|M_q|^2$ and $\eta_q = (e^{\hbar\omega_q/k_BT}-1)^{-1}$ are the phonon energy, the electron–phonon matrix elements and phonon number, respectively, related to the phonon wave vector q. Within the elastic assumption, the self-energy for acoustic–phonons can be reduced to [6]

$$\Sigma^{\lessgtr}_{ac,\nu}(E) = \frac{\Xi^2 k_B T}{\rho u_s^2} G^{\lessgtr}_{\nu}(E), \quad (2)$$

within the scalar deformation potential Ξ approach [9], where ρ is the density and u_s is the sound velocity of silicon. On

978-1-4799-5288-5/14/$31.00 © 2014 IEEE

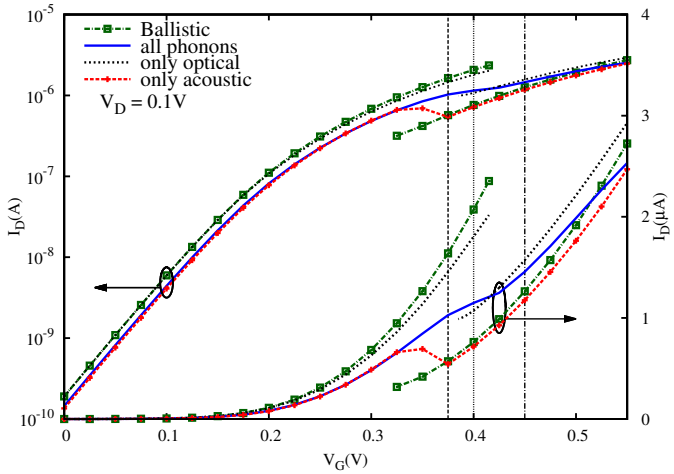

Fig. 2. $I_D - V_G$ characteristics of the nanowire MOSFET of Fig. 1. Four transport regimes are considered: i) ballistic (squares), ii) SCBA with both acoustic and optical phonons (solid line), iii) with optical phonons only (dotted line) and iv) with acoustic phonons only (dashed line with crosses). The vertical dashed, dotted and dash-dotted lines represent the value of V_G=0.375 V, 0.4 V and 0.45 V respectively. $T = 300$ K and V_D=0.1 V.

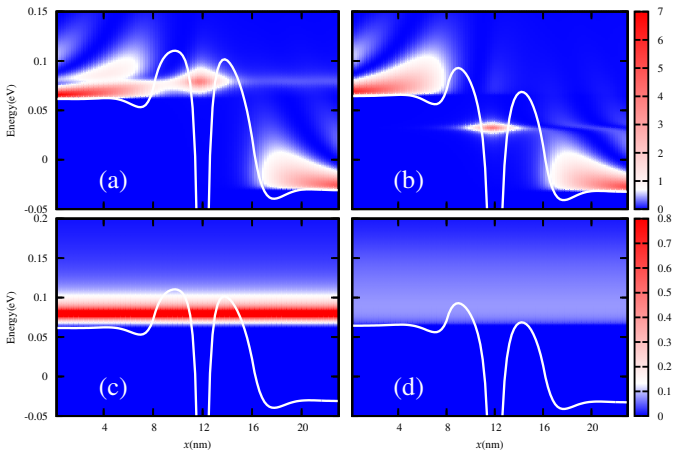

Fig. 3. Ballistic electron density (top) and current (bottom) spectra for the two current points at $V_G = 0.375$ V in Fig 2 (defined by the vertical dashed line). Left column represents the higher branch of the current while right column represents its lower counterpart. The white line is the first subband energy profile along the transport direction. $T = 300$ K and V_D=0.1 V.

the other hand, the optical–phonon scattering self-energy $\Sigma^{\lessgtr}_{j,\nu}$ can be also re-written as [6], [9]

$$\Sigma^{\lessgtr}_{j,\nu}(E) = \frac{\hbar(D_t K_j)^2}{2\rho\omega_{q_j}} \sum_{\nu'=1}^{3} \mathrm{g}_j^{\nu,\nu'} \Big[\eta_{q_j} G^{\lessgtr}_{\nu'}(E \mp \hbar\omega_{q_j}) + (\eta_{q_j}+1) G^{\lessgtr}_{\nu'}(E \pm \hbar\omega_{q_j}) \Big], \quad (3)$$

for the $j-$th optical phonon scattering mechanism with coupling constant $D_t K_j$ and phonon angular frequency ω_{q_j} [9]. The prefactor $\mathrm{g}_j^{\nu,\nu'}$ stands for the selection rule as $\mathrm{g}_j^{\nu,\nu'} = \delta_{\nu,\nu'}$ for g$-$type phonons and $\mathrm{g}_j^{\nu,\nu'} = (1 - \delta_{\nu,\nu'})$ for $f-$type phonons [6].

The electron-phonon matrix elements are calculated using bulk deformation potentials and phonon frequencies from Ref. [5]. Only the imaginary part of the self-energies is considered which stands for including the broadening of the energy levels and neglecting the shift in energy. Convergence criteria of 1% and 0.1 % are applied on the current and the electron density respectively.

Finally, the electron-electron interaction is treated within the Hartree approximation by solving the NEGF transport equations self-consistently with Poisson's equation. In that scheme, the Coulomb potential of the donor is described by adding a positive electron charge on the impurity site in the 3D Poisson equation. Although this approach neglects the chemical nature of the impurity and its short range potential, it correctly describes the long range coulombic tail which is assumed to have the largest impact on the transport.

III. Simulation Results

Fig. 2 shows the drain current *versus* gate voltage characteristics ($I_D - V_G$) obtained at 300 K in four transport regimes: i) the ballistic non-interacting case, ii) with both acoustic and optical phonons, iii) with optical-phonons only and iv) with acoustic-phonons only. We first note that ballistic current depicts a hysteresis from $V_G \simeq 0.32$ V to $V_G \simeq 0.42$ V, confirming the bistability reported by Mil'nikov *et al.* [1]. Figs. 3(a-c) show ballistic electron density and current spectra for the upper branch of the current characteristic at $V_G = 0.375$ V (represented by vertical dashed line in Fig. 2). In this configuration, the dopant level (ϵ_r) is above the source subband energy (ϵ_s) and impurity is mainly screened by electrons of the source. Figs.3(b-d) show the same physical parameters for the lower branch where ϵ_r is now below ϵ_s. The donor is then populated by electrons injected from the drain, leading to a different screening with a strong reduction of broadening of the impurity level.

Interestingly, incorporating all phonon interactions removes the current hysteresis (solid line in Fig. 2). As shown by Figs. 4(a-b) the broadening of the resonant site does not depend anymore on its position with respect to ϵ_s. It results in a smooth

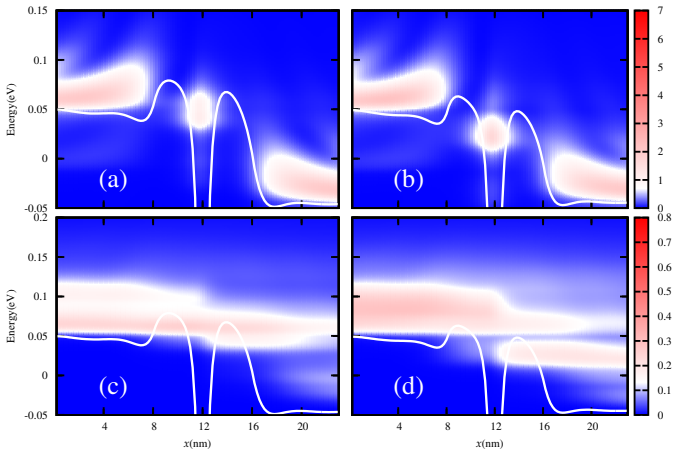

Fig. 4. SCBA electron density (top) and current (bottom) spectra with both acoustic and optical phonons at $V_G = 0.40$ V (a-c) and $V_G = 0.45$ V (b-d)). In each sub-figure, the white line is the first subband energy profile along the transport direction. $T = 300$ K and V_D=0.1 V.

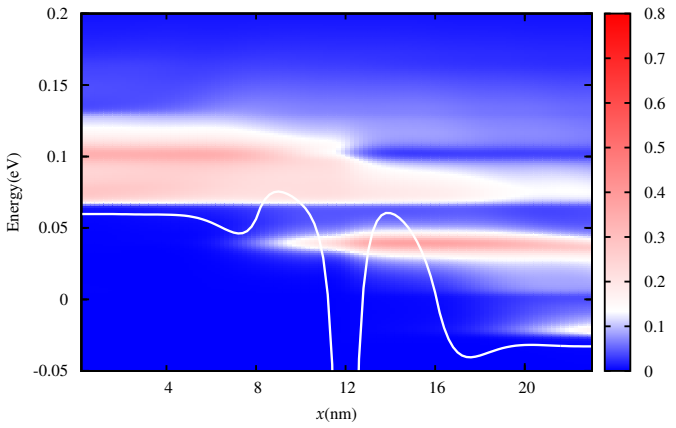

Fig. 5. SCBA current spectrum with only optical phonon interactions at V_G=0.425 V. The component resulting from phonon-assisted resonant tunneling is clearly visible. The white line is the first subband energy profile along the transport direction. $T = 300$ K and V_D=0.1 V.

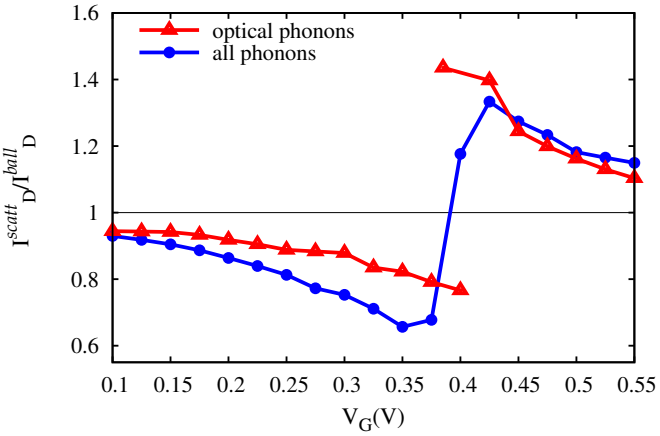

Fig. 6. Ballisticity (I_D^{scatt}/I_D^{ball}) of the nanowire transistor with i) the optical phonons only (triangles), and ii) including all phonon interactions (circles). The current increase at high V_G is clearly ascribable to interactions with optical-phonons. $T = 300$ K and V_D=0.1 V.

transition of the current when ϵ_r goes below ϵ_s at V_G=0.4 V (Figs. 4(c-d)).

Current characteristics including separately acoustic and optical phonons allow to shed light on the scattering influence (Fig. 2). Interestingly, acoustic phonons suppress the hysteresis while their optical counterparts preserve it. At low V_G acoustic phonons have the largest impact on the current decrease. The current obtained with acoustic processes only is almost equal to the one including all the phonon interactions as is the case in undoped systems [10]. We checked that acoustic phonons generate a constant impurity level broadening, $\Gamma_{ac} \simeq 20$ meV ($\simeq \Gamma_{ph}$, with all phonons) for the whole range of gate voltages. The lowering of this broadened level below ϵ_s blocks the resonant transport of source electrons. It then follows a kink in the acoustic phonon current characteristic at V_G=0.35 V which is still visible when both types of phonons are included.

On the other hand, the weaker coupling with optical phonons in nanowires [10] induces less modifications of the electron density. However optical phonons induce electrons relaxation into the donor state at high V_G which results in a phonon–assisted resonant tunneling as shown in Fig. 5. A second "channel of transmission" appears on the current spectra at 65 meV below the ballistic contribution. This characterizes electrons injected from the source that relax into the impurity site by emitting a phonon and subsequently tunnel to the drain side. Phonon–assisted resonant tunneling generates a current even larger than in the ballistic regime up to V_G=0.5 V (Fig. 2).

In order to quantitatively estimate the impact of the phonon–assisted resonant tunneling, Fig. 6 shows the ballisticity obtained with all phonons and optical phonons only. Ballisticity is defined as the ratio of the ballistic current (I_D^{ball}) over the scattering one (I_D^{scatt}) where I_D^{ball} is recalculated with the potential including scattering [7]. We clearly see two regimes with respect to the gate voltage. For $V_G \lesssim 0.4$ V phonon scattering leads to a current reduction (ballisticities are below unity). The important difference between "all phonons" and "optical phonons" simulations demonstrates the impact of acoustic phonon scattering in this gate voltage interval.

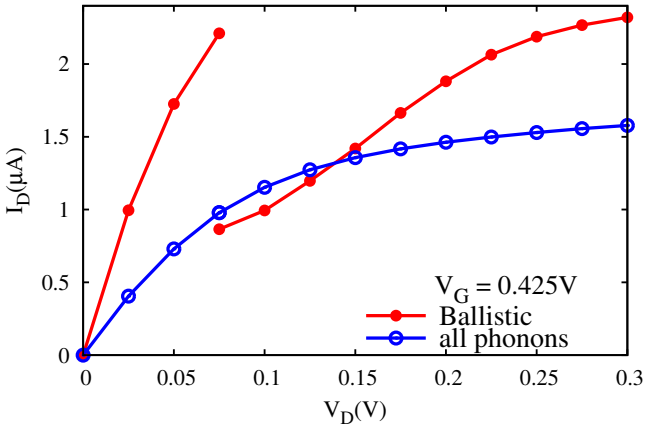

Fig. 7. $I_D - V_D$ characteristics of the nanowire MOSFET in the ballistic regime (full dots), and when all phonon interactions are included (empty dots). V_G=0.425 V. $T = 300$ K.

For $V_G \gtrsim 0.4$ V ballisticities are above unity. The two curves are now close to each other which testifies that optical phonon interactions predominate and that phonon assisted resonant tunneling is the origin of the abrupt current increase. Moreover ballisticities slowly decrease with V_G since multi-phonon processes are required when the resonant energy site ϵ_r is well below ϵ_s.

It is also important to note that similar results can be obtained with $I_D - V_D$ curves by adjusting V_G so that the impurity level is close to ϵ_s (Fig. 7). As for $I_D - V_G$ characteristics, hysteresis effect appears in the ballistic regime and it is removed when phonon scattering is incorporated.

To summarize, acoustic phonon scattering reduces current at low V_G and suppresses the hysteresis, while optical phonons increase the current in the on-regime. However the bi-stability of the system is expected to be recovered at low temperature where acoustic-phonon interactions might be significantly reduced. Moreover the presence of the bistability in output

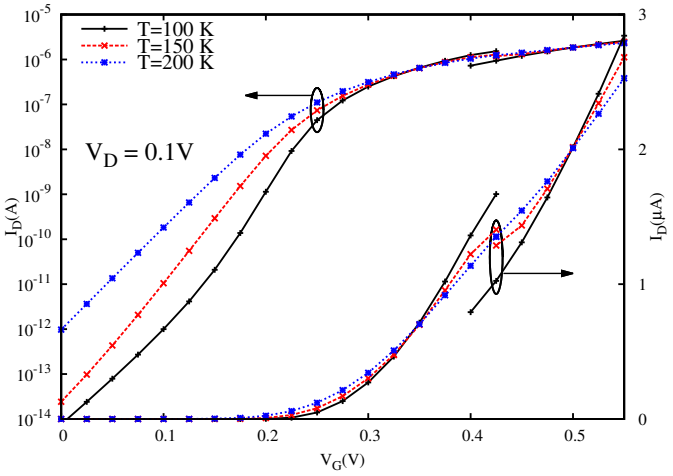

Fig. 8. $I_D - V_G$ characteristics for different temperatures when all phonon scattering are included. We see that the hysteresis is recovered at $T \approx 150$ K. V_D=0.1 V.

characteristics raises an important issue for technological applications. For instance hysteresis might be used for resistance switching memories which are realized so far with planar resonant tunneling diodes [11]. We then calculate the impact of temperature on the current characteristics for intermediate temperatures ($T >$100 K).

Fig. 8 represents current characteristics at different temperatures considering the self-energies interactions of Eqs.(2) and (3). We find that the bistability is restored around 150 K. This is mainly due to the linear temperature dependence of the self-energy of the acoustic phonon interactions (Eq.(2)) which are at the origin of the hysteresis lifting. Unfortunately validity of Eq.(2) is restricted to relatively high temperature calculations where phonon frequencies are much smaller then thermal energy. For low temperatures, we can show [12] that dependence of the self-energy is no longer linear. Starting from the general expression of Eq.(2) and considering energies close to the localized state ϵ_r, the self-energy of acoustic phonons near the impurity can be expressed as:

$$\Sigma^{\lessgtr,IMP}_{ac,\nu}(E) = \frac{\Xi^2}{2\rho u_s^2} G^{\lessgtr}_{\nu}(E) \times \frac{3}{4}\hbar\omega_c, \qquad (4)$$

where ω_c is the critical frequency below which the self-energy becomes temperature independent. In the case of silicon, this frequency corresponds to an effective critical temperature $T_C \approx 90$ K which generates a small enough level broadening to obtain the bistability (Fig. 8). This makes us assume that the hysteresis will be restored when decreasing the temperature around 150 K. Further developments are however required to confirm this point.

IV. Conclusion

The effects of both acoustic and optical phonon interactions on a single dopant nanowire MOSFET have been analyzed. Based on a 3D non-equilibrium Green's function approach, we showed that i) phonon scattering suppresses the current hysteresis at room temperature; ii) the strong acoustic phonon coupling in nanowires is responsible of this suppression; iii) contrary to undoped nanowire devices, optical phonons have an important impact on the on-current. They induce an assisted resonant tunneling through the impurity level, resulting in a significant current increase. Finally considering a linear temperature dependence of the acoustic phonon self-energy, we showed that the current hysteresis should be restored at 150 K. Our analytic developments showed that this linear dependence remains valid down to a critical temperature $T_C \approx$90 K. Below this value acoustic phonon self-energy should not decrease anymore. Therefore hysteresis might be restored by cooling down the system. Additional work is however under progress to assess the importance of other strong approximations used in our description of the electron-phonon self-energies, especially concerning the bulk deformation potentials and the local description of the interactions.

Acknowledgment

This work is supported by the QUASANOVA and SIMPSSON contracts funded by the ANR-French National Research Agency.

References

[1] G. Mil'nikov, N. Mori, Y. Kamakura, and T. Ezaki, *Phys. Rev. Lett.*, vol. 102, p. 036801, 2009.

[2] B. Roche, R.-P. Riwar, B. Voisin, E. Dupont-Ferrier, R. Wacquez, M. Vinet, M. Sanquer, J. Splettstoesser, and X. Jehl, *Nat. Commun.*, vol. 4, p. 1581, 2013.

[3] M. Bescond, M. Lannoo, L. Raymond, and F. Michelini, *J. Appl. Phys.*, vol. 107, p. 093703, 2010.

[4] N. Wingreen, K. Jacobsen, and J. Wilkins, *Phys. Rev. Lett.*, vol. 61, p. 1396, 1988.

[5] M. Bescond, C. Li, H. Mera, N. Cavassilas, and M. Lannoo, *J. Appl. Phys.*, vol. 114, p. 153712, 2013.

[6] S. Jin, Y. J. Park, and H. S. Min, *J. Appl. phys.*, vol. 99, p. 123719, 2006.

[7] M. Luisier and G. Klimeck, *Phys. Rev. B*, vol. 80, p. 155430, 2009.

[8] N. D. Akhavan, I. Ferain, R. Yu, P. Razavi, and J. P. Collinge, *J. Comp. Electron.*, vol. 11, p. 249, 2012.

[9] C. Jacoboni and L. Reggiani, *Rev. Mod. Phys.*, vol. 55, p. 645, 1983.

[10] M. Aldegunde, A. Martinez, and J. R. Barker, *J. Appl. Phys.*, vol. 113, p. 014501, 2013.

[11] J. Denda, K. Uryu, K. Suda, and M. Watanabe, *Appl. Phys. Express*, vol. 7, p. 044103, 2014.

[12] M. Lannoo and M. Bescond, *unpublished*, 2014.